# Influence of stress on optical transitions in GaN nanorods containing a single InGaN/GaN quantum disk

Y. D. Zhuang<sup>1</sup>, J. Bruckbauer<sup>2</sup>, P. A. Shields<sup>1</sup>, P. R. Edwards<sup>2</sup>, R. W. Martin<sup>2</sup>, D. W. E. Allsopp<sup>1\*</sup>

<sup>1</sup> Dept. of Electronic and Electrical Engineering, University of Bath, Bath, BA2 7AY, UK

<sup>2</sup> Dept. of Physics, SUPA, University of Strathclyde, Glasgow, G4 0NG, UK

\* Corresponding author, e-mail: d.allsopp@bath.ac.uk

**Abstract.** Cathodoluminescence (CL) hyperspectral imaging has been performed on GaN nanorods containing a single InGaN quantum disk (SQD) with controlled variations in excitation conditions. Two different nanorod diameters (200 and 280 nm) have been considered. Systematic changes in the CL spectra from the SQD were observed as the accelerating voltage of the electron beam and its position of incidence are varied. It is shown that the dominant optical transition in the SQD varies across the nanorod as a result of interplay between the contributions of the deformation potential and the quantum-confined Stark effect to the transition energy as consequence of radial variation in the pseudomorphic strain.

Keywords: Enter Keywords here.

PACS: Replace this text with PACS numbers; choose from this list: http://www.aip.org/pacs/index.html

#### 1. Introduction

Group III—nitride nanorods have attracted wide interest as a vehicle for studying their fundamental material properties<sup>1</sup> as well as for their potential application in high brightness light emitting diodes<sup>2–10</sup>. Compared with other III-V semiconductors the III—nitrides show strong polarization especially along the c-axis with the effect that strain can have a major influence on the optical properties in  $In_xAl_yGa_{1-x-y}N$  based quantum wells  $(QWs)^{11}$ . The formation of a nanorod structure, either by bottom-up epitaxial growth<sup>2–5</sup> or by dry etching a pre-existing epitaxial III—nitride layer<sup>6–10</sup>, has been proposed as a means of alleviating strain due to the free surface presented by the sidewalls enabling the lattice to relax<sup>12–14</sup>.

In the case of homogeneous nanorods formed by dry etching from *c*-plane homo-epitaxial GaN templates, the degree of strain relaxation in the overall structure will depend on the diameter and height of the nanorods, with complete strain relaxation occurring when their height exceeds their diameter irrespective of the type of substrate used<sup>15</sup>. When such etched nanorods contain an InGaN QW or a MQW oriented in the *c*-plane changes in the optical transition energy have been observed and are frequently ascribed to the impact of the strain relaxation in the nanorod on the piezoelectric contribution to the quantum-confined Stark effect (QCSE)<sup>9</sup>. However, several theoretical studies have revealed that the effect of the distribution of the pseudomorphic strain and the concomitant polarization variation is more complex<sup>13, 16</sup>. One theoretical study has predicted not

only the widely-observed line shifts associated with the QCSE, but also multiple transitions associated with electrons and holes being localized in different positions across the radius of the nanorod<sup>13</sup>. Recently evidence has emerged to support these predictions<sup>17</sup>, but a comprehensive measurement-based study is still required to identify the combined influences of the effects of axial and radial strain on light emission from c-plane oriented QWs, notably contributions to transition energies from the bulk deformation of the InGaN layer(s) and the QCSE.

This paper reports a detailed study of optical transitions in isolated, nominally fully relaxed GaN nanorods containing a single pseudomorphic InGaN QW by cathodoluminescence (CL) hyperspectral imaging. The CL system used combines high spectral resolution with high spatial resolution, to provide positional information about the location of the observed optical transitions on a scale much smaller than the diameter of the nanorods <sup>18, 19</sup> and is therefore able to track changes in the luminescence associated with both radial and axial strain variations in the nanorods. The paper is organized as follows. Section 2 presents an overview of the structure of nanorods, the methods used in their fabrication and the CL hyperspectral imaging system. Section 3 presents a detailed description and discussion of the results and the conclusions of the work are given in section 4.

## 2. Sample fabrication

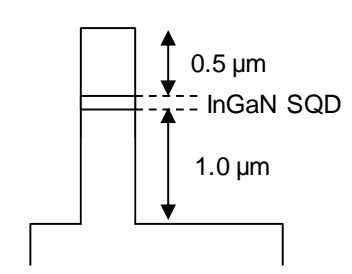
The nanorods used in this research were fabricated by post-growth processing of a GaN epitaxial structure containing a single c-plane oriented InGaN QW grown by metal organic chemical vapor deposition. The epitaxial structure, starting from the sapphire substrate, comprised a 4  $\mu$ m n-type GaN:Si layer, followed by a ~2 nm wide InGaN single QW (emission wavelength  $\approx 440$  nm) and capped by a 0.5  $\mu$ m p-type GaN:Mg layer.

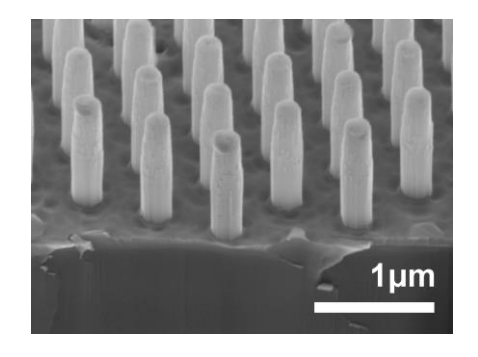
The nanorods were formed using a combined nano-imprint lithography/lift-off technique<sup>20</sup> to define a hexagonal array (600 nm pitch) of relatively thick ( $\sim$ 100 nm), 300 nm diameter nickel nano-dots to act as a dry etch mask. Nanorods of height  $\sim$ 1.5 µm were then formed by inductively-coupled plasma (ICP) etching in Cl<sub>2</sub> and Ar at a temperature of 150°C, a process that produces high aspect ratio nanorods with vertical sidewalls<sup>20</sup>. The damaged layer on the nanorod sidewalls introduced by ICP etching was removed by etching in KOH at 40°C to produce an ordered array of regular shaped nanorods containing a single disk-shaped QW lying in the c-plane that emit strong photoluminescence (PL) at room temperature. Arrays of nanorods of different diameter (range 120–280 nm) were fabricated by cleaving the sample after ICP etching and then adjusting the

duration of the KOH etching step. Single nanorods were formed for CL hyperspectral imaging by carefully cleaving some of the nanorods at their base from the underlying GaN layer.

### 3. Results and discussion

The upper part of Fig. 1 shows a schematic of the nanorod structure in which the 2 nm thick InGaN layer extends across the whole diameter to form in effect a single quantum disk (SQD). The middle part of Error! Reference source not found. shows a secondary electron (SE) image of an array of such nanorods and the lower shows the variation with diameter of the PL room temperature PL emitted from each array of nanorods. The QW PL from the un-etched starting planar material is characterized by a single emission peak centered at 460 nm (not shown). On etching the nanorods, the SQD emission spectra of the various nanorods is progressively blue shifted as the diameter is reduced from 280 nm to 200 nm with little further shift with further reduction in diameter down to 120 nm. A second feature of the SQD is a broadening of the emission peak caused by the emergence of a second transition close in energy, this occurring irrespective of the nanorod diameter. Similar broadening associated with a second transition has been observed in low temperature micro PL performed on isolated nanorods fabricated in the same way from nominally the same planar epitaxial structure<sup>21</sup>. The lower energy of these two transitions was found to have a long decay constant, indicating that the recombining carriers were spatially separated within the SQD<sup>21</sup>.





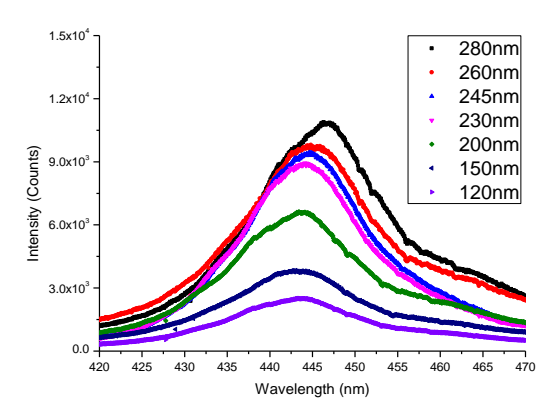


Fig. 1 (a) Schematic of the nanorod structures containing a SQD; (b) SE image of an array of InGaN/GaN SQD nanorods with an average diameter of 280 nm and (c) variation with nanorod diameter in the room temperature SQD PL (inset: nanorod diameters).

CL hyperspectral imaging was performed in a field emission gun scanning electron microscope (FEI Sirion 200) modified for CL spectroscopy. An advantage of the hyperspectral imaging system used is its ability to measure shifts in emission wavelength on a length scale < 20 nm<sup>22</sup>, thus enabling precise mapping of CL spectral features. The CL was excited with an electron beam with accelerating voltage of 2 kV, 10 kV or 30 kV, with the sample held at room temperature. Increasing the accelerating voltage increases the penetration depth of the electron beam and, for a fixed electron beam current, causes a much slower reduction in the spot size illuminated by the beam. Thus, the use of different accelerating voltages enables the impact of progressively increases in the penetration depth of the electron beam into the nanorod at different axial positions on the CL to be resolved. In this way axial and radial variations in strain on the CL could be determined.

The magnitude of the beam current on the spatial resolution achieved by varying the beam conditions must be taken into account. For most measurements the beam current was held at 2 nA. Some measurements with a 10 kV beam were repeated for beam currents of 0.5 and 0.1 nA to investigate the extent to which the excited charge carriers screen the polarization in the SQD. Table 1 shows the estimated electron beam spot sizes under the different experimental conditions used.

Accelerating voltage	2 kV	10 kV	30 kV
Spot size for 2.1 nA beam current	10 nm	7 nm	4 nm
Spot size for 0.5 nA beam current		3.5 nm	
Spot size for 0.1 nA beam current		2 nm	

Table 1 Estimated electron beam spot sizes.

Measurements were performed on both standing and felled nanorods, the latter formed by carefully cleaving the nanorods at their base from the underlying GaN layer. Two nanorod diameters were studied in detail: 280 nm and 200 nm, the latter being the minimum diameter for which variations in the SQD PL was observed. In the case of felled nanorods the incident electron beam was scanned in a plane parallel to their long axis through the SQD starting and ending in the GaN layers above and below. For standing nanorods the electron beam was incident at an angle of ~45° to the nanorod sidewalls.

The CL spectrum at each point in the beam scan was dispersed by a spectrograph and recorded by an electron multiplying charge coupled device (EMCCD) to obtain multi-dimensional datasets combining both spectral and positional information.<sup>18</sup> The measured spectra were smoothed using a high frequency filtering algorithm to remove noise introduced by the EMCCD.

Fig. 2 shows (a) the SE image of a <u>single</u> felled nanorod, and CL intensity maps of (b) the GaN band edge emission and (c) the SQD emission, all obtained at an accelerating voltage of 30 kV and beam current of ~2 nA, which produced a calculated beam spot size of ~4 nm. Scanning the nanorod with a beam of this size enables the CL emission spectra to be correlated to small volumes of the nanorod, enabling CL images to be extracted by post-processing a single hyperspectral image dataset. The CL from the SQD is intense in comparison to the GaN band edge emission, with the latter only observed from below the SQD (right-hand side of the nanorod) owing to the p-type doping of the GaN layer above the InGaN SQD.

The peak energy of the GaN band edge CL was almost unchanged with the point of incidence of the electron beam position on the GaN layer below the InGaN SQD for all three accelerating voltages used; i.e. it was independent of beam penetration depth. This was the case for both standing and felled nanorods. Further, the peak energy of this GaN band edge CL correlated with that of unstrained material, from which it can be inferred that the GaN sections of the nanorods wires were relaxed to a depth of > 100 nm. The results conforms with an earlier finding that virtually complete strain relaxation occurs in GaN nanorods with a height-to-diameter ratio > 1 formed from continuous c-plane layers by essentially the same lithographic and dry etching process<sup>23</sup>. Further, it can also be inferred that any strain in the InGaN layer derives purely from lattice mismatch strain arising from pseudomorphic growth.

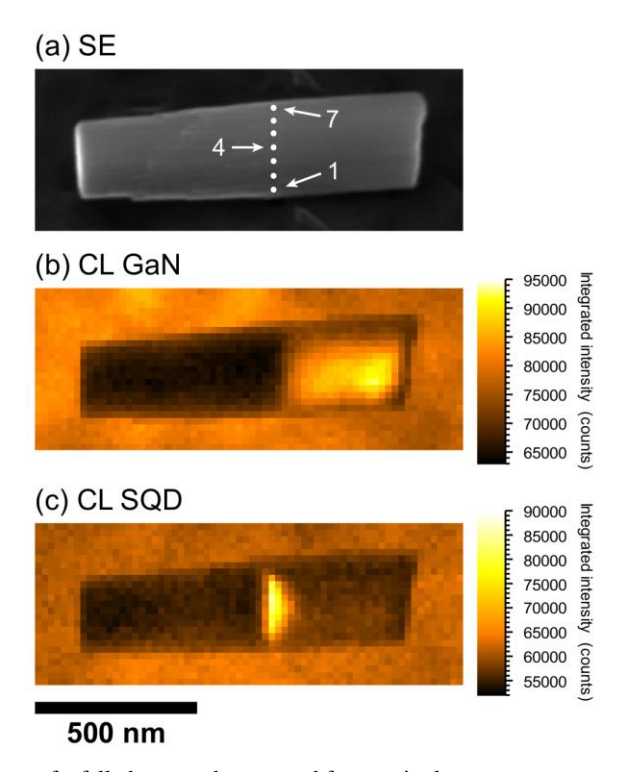


Fig. 2 Monochromatic CL intensity maps of a felled nanorod, extracted from a single room-temperature CL hyperspectral image obtained at 30 kV: (b) integrated emission over spectral range 345–390 nm (GaN band edge emission) and (c) integrated emission over spectral range 410–475 nm (InGaN SQD emission). The corresponding SE image is also shown (a) with the top of the nanorod on the left-hand side. The line of white dots with numbers in the SE image marks the two edges (position 1 and 7) and the center (position 4) of the SQD emission.

Fig. 3(a) shows the spectral variation of the SQD emission taken from selected line-scans in the hyperspectral image obtained from the same nanorod at the same accelerating voltage and beam current at the positions indicated in Fig. 2(a) by the line of white dots. Several felled nanorods of the same diameter were investigated in the same way and the following results are typical. As the beam traverses across the InGaN SQD, the CL emission band evolves from being dominated by a single peak at ~2.78 eV at the sidewall of the nanorod (point 1) to being double peaked as a second peak at ~2.84 eV progressively emerges as the excited area moves toward the center of the rod (points 2, 3, and 4). At the center of the InGaN SQD the peak at ~2.84 eV dominates, and the evolution in the CL spectrum is reversed as the electron beam traverses to the other sidewall of the nanorod (points 5, 6 and 7).

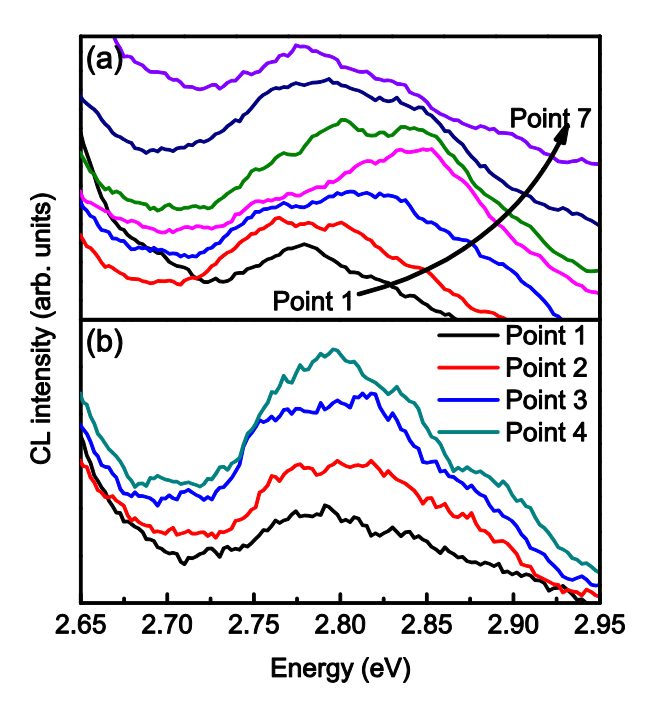


Fig. 3 (a) InGaN SQD emission spectra as a function of lateral position in the InGaN SQD in a "felled" 280 nm diameter nanorod, and (b) position dependent CL spectra of a "standing" nanorod of the same diameter. Both data sets were obtained at 30 kV and 2 nA beam current.

Fig. 3(b) shows the positional evolution, from edge-to-center, of the CL from the InGaN SQD excited by a 30 kV electron beam in a standing nanorod on the same sample. The pattern is similar to that for a felled nanorod with the higher energy peak emerging at the same position to within 1 meV when the electron beam is aligned to the center of the nanorod, although the intensity of the peak at ~2.84 eV is less pronounced. The likely reason for this is the different angles of incidence of the electron beam for the felled and standing nanorods. For standing nanorods the electron beam is incident at an angle to the longitudinal axis of the nanorod, whereas for felled nanorod it is more aligned to the plane of the quantum well. The latter results in stronger excitation of the SQD, notably its inner core, evidenced by higher signal to noise ratio in Fig. 3a. Otherwise, the trends in the width and general shape of the spectra with position of entry of the electron beam from positions 1 through to 4 are the same for the felled and standing nanorods. Also, a second higher energy emission peak at ~2.88 eV is also now resolved when the beam is aligned with the center of the SQD. The overall effect of the emergence and growth of the ~2.84 eV peak is to cause an apparent blue shift in the SQD emission peak and to increase its full width half maximum (FWHM) as the electron beam was scanned from edge to center of the InGaN disk. On continuing the scan to the opposite edge of the nanorod the evolution of the line shape is reversed.

Changing the accelerating voltage caused systematic changes in the CL spectra. Fig. 4 shows the impact on the CL across the SQD in a felled nanorod after reducing the accelerating voltage to 10 kV. The beam current was again ~2 nA, which for

this beam voltage and current produced a beam spot size of ~7 nm diameter at the sample surface. The apparent blue shift in the SQD emission peak as the electron beam is scanned from edge to center is still observed at this lower beam voltage. (Points 1–7 correspond to those shown in Fig. 2(a)). However, the double-peak nature of the CL from the SQD is no longer clearly resolved and is evident only in a marked asymmetry in the emission band from the center of the nanorod (point 4). The symmetry in the edge-to-edge evolution of the SQD emission band with position of the electron beam, notably the apparent shift in its peak energy, is now obvious.

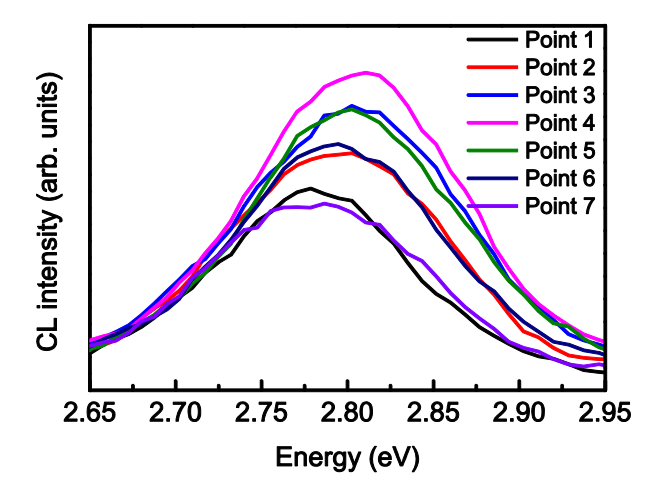


Fig. 4 Evolution with lateral position of the CL excited by an electron beam of accelerating voltage of 10 kV and 2 nA current from an identical felled GaN nanorod containing an InGaN SQD from the edge (points 1 and 7) to the center (point 4).

Possible contributions to the spectral changes from the QCSE and from band filling were investigated by varying the beam current, and hence the densities of induced electron-hole pairs, at a constant accelerating voltage of 10 kV. The results from CL collected from the center of the InGaN SQD are shown in Fig. 5. Increasing the beam current causes a red shift in the CL indicating that neither screening of the QCSE nor band filling plays a significant role in the observed spectral shifts with beam position shown in Figs. 3 and 4, as both would be expected to cause a blue shift. A temperature rise caused by increasing beam current can also be discounted as the mean position of the CL emission spectra shown in Figures 3 and 4 is unchanged as the accelerating voltage, hence energy input to the nanorods, is increased by a factor three (from 10 to 30 kV). Rather, the changes in the CL spectra derive from position and accelerating voltage dependent excitation of two or more emission peaks within the SQD.

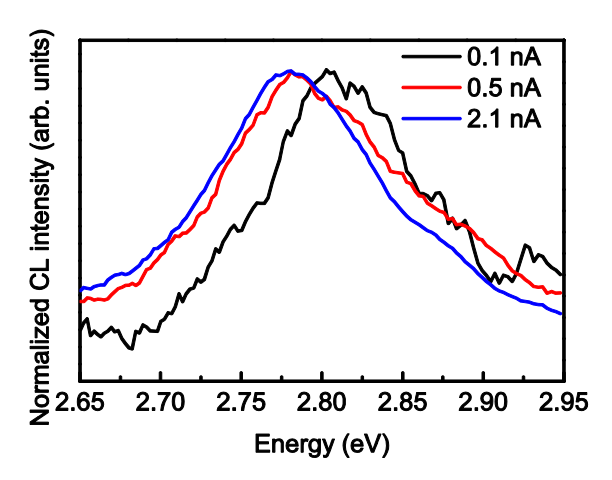


Fig. 5 Normalized CL spectra from the center of the InGaN SQD excited for three different nominal beam currents with the accelerating voltage held constant at 10 kV.

It has been shown that a radial strain gradient exists across the InGaN layer from its center to edge with its outer shell largely relaxed <sup>14, 24</sup>. As such and noting that increasing the accelerating voltage of the electron beam increases its penetration depth into the nanorods, the changes in the observed CL with electron beam position and accelerating voltage should reflect the strain variation across the SQD.

In order to determine more precisely the changes in excitation volume with electron beam parameters, Monte Carlo simulations of the electron trajectories within a GaN layer were performed for accelerating voltages of 2, 10 and 30 kV using CASINO<sup>25</sup>. The resulting calculations of effective excitation volume for different electron beam alignments can then be correlated with the changes in the CL spectra. Fig. 6 shows plots of the electron deposition profiles calculated from these trajectories for beam voltages of 2, 10 and 30 kV. Cross-sections of a 280 nm diameter nanorod with an assumed 20 nm wide shell in which strain is reduced have been superimposed on these electron profiles in positions corresponding to points 1 (edge) and 4 (center) in Fig. 3 and Fig. 4, to show how varying the alignment of the electron beam and its accelerating voltage enables building an excitation map of the SQD.

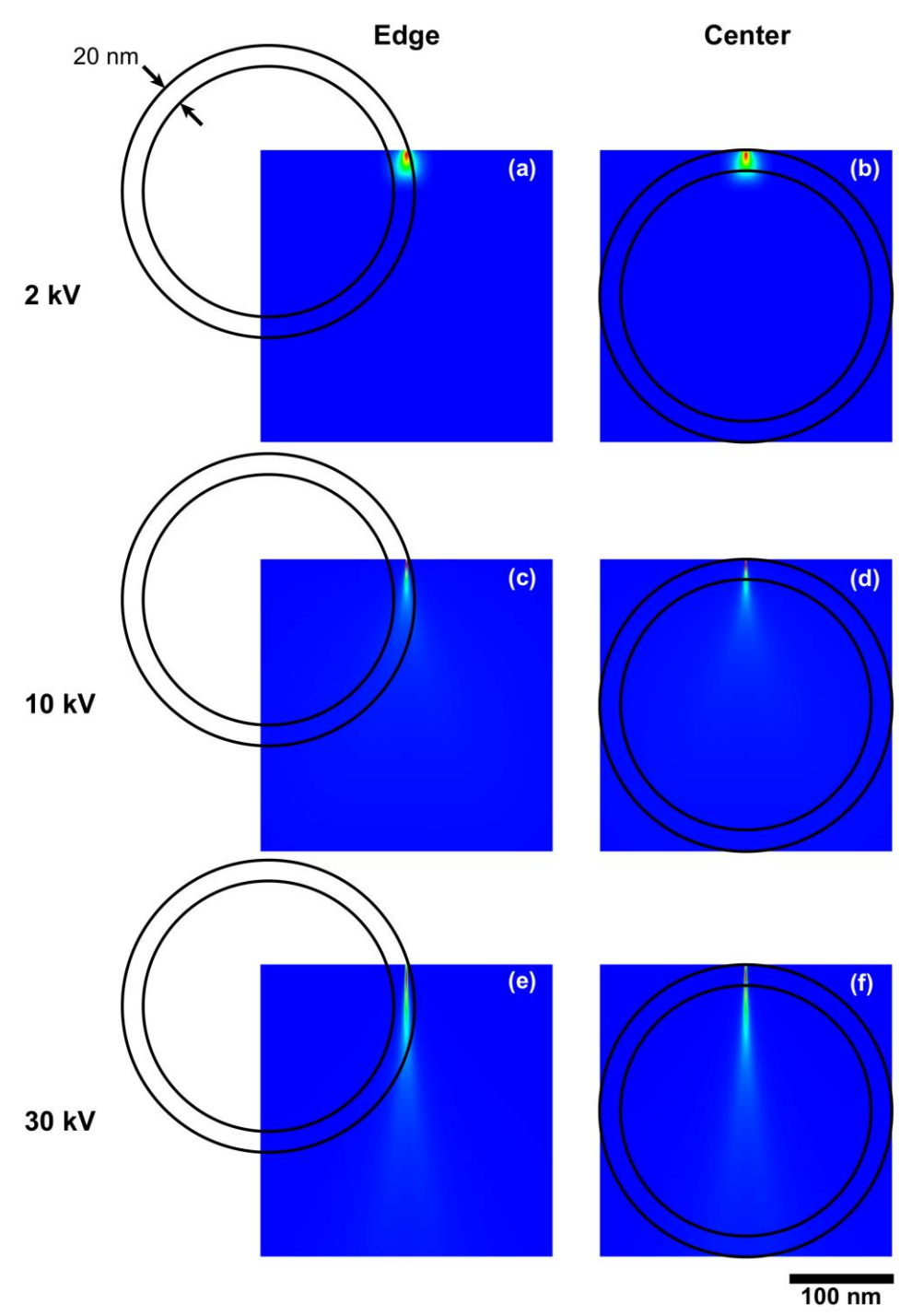


Fig. 6 Energy deposition profiles from Monte Carlo electron trajectory simulations for (a, b) 2 kV, (c, d) 10 kV and (e, f) 30 kV beams impinging on a GaN sample overlaid with cross sections of SQDs of a felled 280 nm nanorod containing a 20 nm fully relaxed outer shell material and strained inner core material.

For example, Fig 6(a) shows that CL excited by a 2 kV beam derives only from a ~25 nm wide outer shell of the SQD irrespective of its alignment. At the other extreme, a 30 kV beam will penetrate ~120 nm into the nanorod with the excitation

volume slowly widening from < 5 nm at the surface to ~15 nm at penetration depth of 120 nm. When aligned to the edge of the nanorod there is strong excitation of the outer shell and some excitation of the core owing to the lateral beam spreading. On the other hand when centrally aligned a 30 kV beam will strongly excite a significant fraction of the SQD core whilst still exciting part of the outer shell, with the effect that the CL spectrum will be more representative of the core. For the 10 kV beam, the shape of the CL spectra should lie between these two extremes with the outer shell making a more dominant contribution for all beam alignments than in the case of the 30 kV beam, but with emission from the core still contributing except when the electron beam is aligned to the edge (beam positions 1 and 7 in Fig. 2a).

Fig. 7 shows a comparison of the normalized CL intensity from (a) the edge and (b) the center of the same nanorod excited by electron beams of 2 kV, 10 kV and 30 kV. The emission peaks of the three spectra taken from the edge of the nanorod coincide closely in energy at ~2.78eV, with the 10 kV and 30 kV spectra somewhat broadened compared with that excited by the 2 kV beam, indicating that some emission from the core does contribute to the spectra but not much in the case of the 10 kV beam. On the other hand, the CL spectra from the center of the InGaN SQD excited by the 10 kV and 30 kV beams are noticeably blue shifted with respect to the 2 kV beam spectrum, which is almost unchanged from that taken from the edge of the SQD.

Taking these data together with the calculations of beam penetration in Fig. 6, it is inferred that the spectrum excited by the 2 kV beam, with its emission peak at ~2.78eV, originates from the outer shell of the SQD. The width of this shell is estimated from the penetration depth of the 2 keV electron beam to be ~25 nm, a value very similar to the calculated width (~20 nm) of the strain-relaxed layer of a freestanding nanorod of height greater than its diameter<sup>4, 24</sup>; from which it is concluded that the ~2.78eV transition originates from strain-free material.

Further, the spectra in Fig. 7 taken together with the energy deposition profiles in Figs. 6(d) and 6(f) for the 10 and 30 keV electron beams show that broadening of the CL peak by ~10–15 meV to higher energy derives from excitation of transitions in the nanorod core, notably that at ~2.84 eV observed in the spectra in Fig. 3. The degree of broadening and the resolution of the contributing emission peaks in the spectrum will depend on the relative excitation of the core and outer shell of the SQD by the electron beam. When aligned to the edge of the nanorod the difference in penetration depth of the 10 and 30 keV beams has little effect on the degree of excitation of the core and the spectra in both cases are dominated by the emission at ~2.78 eV from the outer shell. However, when the beams are aligned with the center of the nanorod, the greater penetration depth of the 30 keV electrons will cause relatively more excitation in the core than a 10 kV electron beam. This has the effect that the CL spectrum will contain a significantly stronger contribution from the ~2.84 eV transition, as observed. On the other hand, CL

spectra excited by the 10 keV beam comprise both emission peaks with a comparatively small change in the relative intensity of the ~2.78 eV and ~2.84 eV peaks as the beam scans from the edge to the center of the InGaN SQD. As a consequence, the CL spectrum appears broadened with the ~2.84 eV peak unresolved, as seen in Fig. 4.

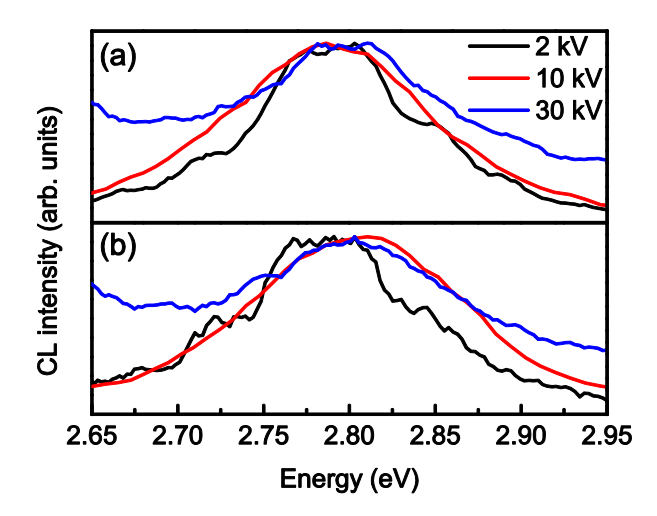


Fig. 7 Comparison of the normalized CL spectra from (a) the edge and (b) from the center of the InGaN SQD by electron beams of 2, 10 and 30 kV accelerating voltage.

Taken as a whole, the data conform to a model in which the observed systematic changes in the CL emitted from the SQD arise from interplay between the QCSE and the deformation potential contribution to the transition energy as the pseudomorphic strain varies from its center to its edge. The QCSE contributes a blue shift in the ground state intersubband transition of the SQD moving from its core to its outer shell as the piezoelectric polarization decreases owing to the strain relaxation at the sidewall. Simultaneously the deformation potential contribution to the InGaN/GaN band gaps decreases as pseudomorphic strain is released at the outer edge of the nanorod, giving rise to a more dominant red shift moving from center to edge<sup>13</sup>. Based on the correlation between the results of Monte Carlo simulations and the hyperspectral CL data the width of relaxed outer shell is ~25nm, consistent with earlier estimates<sup>14, 24</sup>.

Finally, the impact of reducing the diameter of the nanorods has been considered. Fig. 8 shows CL spectra measured at five points across a SQD in a 200 nm diameter nanorod, obtained with an electron beam current of 130 pA and 10 kV accelerating voltage. Only five measurement points were considered in the thinner nanorods: points 1 and 5 correspond to the two edges of the SQD, point 3 lies at its center and point 2 (4) lies approximately mid-way between points 1 (5) and 3. Since the width of the relaxed outer shell will be independent of nanorod diameter<sup>7</sup> the impact of reducing the nanorod diameter will be to

increase the contribution of the outer shell contributes to the volume excited by the electron beam relative to that contributed by the strained inner core. Thus, the lower energy CL peak ( $\sim$ 2.78 eV) will be more dominant in the spectrum than the emission at  $\sim$ 2.84 eV from the strained nano-disk core, as observed in Fig. 8, to provide further evidence for the interplay between bulk deformation and the QCSE in determining the optical transition energies in pseudomorphic c-plane oriented InGaN QWs in GaN nanorods. The net effect of this interplay is for the lower energy transition energy to occur in the relaxed outer shell of the SQD, with possible Fermi level pinning at the SQD surface making the transition spatially indirect<sup>14, 24</sup>.

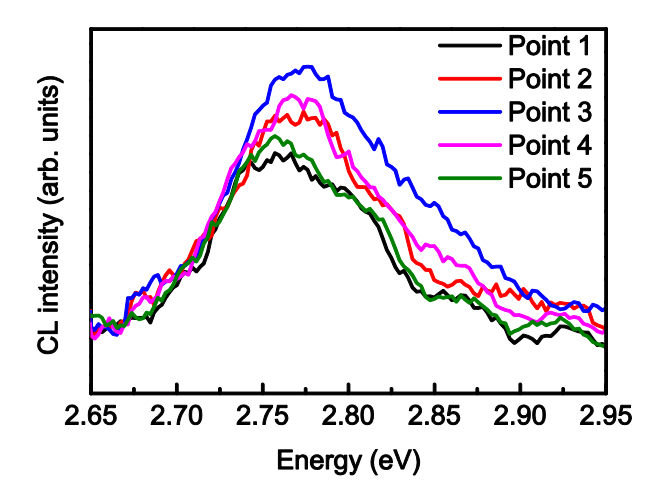


Fig. 8 (a) CL spectra measured at five points across an InGaN SQD embedded in a 200 nm diameter felled nanorod. Points 1 and 5 correspond to the edge and point 3 to the center of the nanorod.

#### **SUMMARY**

CL hyperspectral imaging and Monte Carlo simulations of the electron excitation volume have been performed on an InGaN SQD embedded in GaN nanorods formed by post-growth nanoimprint lithography and ICP etching. The measurements were performed for nanorods of 280 nm and 200 nm diameter and for different accelerating voltages and beam currents. In all cases the CL spectra contained two peaks which are shown to be associated with a radial variation in the ground state QW transition in such a way that two distinct optical transitions closely spaced in energy occur at different radial positions in the nano-disk. This behavior is explained by the opposing impacts of the QCSE and the deformation potential contributions to the transition energy with the radial strain variation from the center to edge of the InGaN SQD.

#### Acknowledgements

The Authors wish to thank Osram for kindly providing the single quantum well epitaxy and Chris Chan of the University of

Oxford, England, for his help in performing the micro-photoluminescence measurements.

#### References

- <sup>1</sup> F. A. Ponce and D. P. Bour, Nature **386**, 351 (1997).
- <sup>2</sup> H.-M. Kim, Y.-H. Cho, H. Lee, S. I. Kim, S. R. Ryu, D. Y. Kim, T. W. Kang, and K. S. Chung, Nano Lett. **4**, 1059 (2004).
- <sup>3</sup> H.-W. Lin, Y.-J. Lu, H.-Y. Chen, H.-M. Lee and S. Gwo, Appl. Phys. Lett. **97**, 073101 (2010).
- <sup>4</sup> W. Guo, M. Zhang, A. Banerjee, and P. Bhattacharya, Nano Lett. **10**, 3355 (2010).
- <sup>5</sup> S. Li and A. Waag, J. Appl.Phys. **111**, 071101 (2012).
- S. Keller, C. Schaake, N. A. Fichtenbaum, C. J. Neufeld, Y. Wu, K. McGroddy, A. David, S. P. DenBaars, C. Weisbuch, J. S. Speck, and U. K. Mishra, J. Appl. Phys. 100, 054314 (2006)
- <sup>7</sup> C. H. Chiu, T. C. Lu, H.W. Huang, C. F. Lai, C. C. Kao, J. T. Chu, C. C. Yu, H. C. Kuo, S. C. Wang, C. F. Lin and T. H. Hsueh, Nanotechnology **18**, 445201, (2007).
- <sup>8</sup> Q. Li, K. R. Westlake, M. H. Crawford, S. R. Lee, D. D. Koleske, J. J. Figiel, K. C. Cross, S. Fathololoumi, Z. Mi, and G. T. Wang, Optics Express 19, 25528 (2011),
- <sup>9</sup> J. Bai, Q. Wang, and T. Wang, J. Appl. Phys. **111**, 113103 (2012).
- <sup>10</sup> Y. D. Zhuang, C. J. Lewins, S. Lis, P. A. Shields, and D. W. E. Allsopp, IEEE Photonics Technol. Lett. 25, 1047 (2013).
- <sup>11</sup> S. Nakamura, T. Mukai, and M. Senoh, Appl. Phys. Lett. **64**, 1687 (1994).
- <sup>12</sup> Y. Kawakami, S. Suzuki, A. Kaneta, M. Funato, A. Kikuchi, and K. Kishino, Appl. Phys. Lett. 89, 163124 (2006).
- <sup>13</sup> C. Böcklin, R. G. Veprek, S. Steiger, and B. Witzigmann, Physical Review B 81, 155306 (2010).
- <sup>14</sup> M. J. Holmes, Y. S. Park, X. Wang, C. C. S. Chan, A. F. Jarjour, R. A. Taylor, J. H. Warner, J. Luo, H. A. R. El-Ella and R. A. Oliver, J. Appl. Phys. **109**, 063515 (2011).
- W. J. Tseng, M. Gonzalez, L. Dillemans, K. Cheng, S. J. Jiang, P. M. Vereecken, G. Borghs, and R. R. Lieten, Appl. Phys. Lett. 101, 253102 (2012).
- <sup>16</sup> C. Rivera, U. Jahn, T. Flissikowski, J. L. Pau, E. Muñoz, and H. T. Grahn, Physical Review B 75, 045316 (2007).
- <sup>17</sup> Y. D. Zhuang, S. Lis, J. Bruckbauer, S. E. J. O'Kane, P. A. Shields, P. R. Edwards, J. Sarma, R. W. Martin and D. W. E. Allsopp, Jpn. J. Appl. Phys. **52**, 08JE11 (2013).
- <sup>18</sup> P. R. Edwards, L. K. Jagadamma, J. Bruckbauer, C. Liu, P. Shields, D. Allsopp, T. Wang, and R. W. Martin, Microscopy and Microanalysis **18**, 1212 (2012).
- <sup>19</sup> J. Bruckbauer, P.R. Edwards, J. Bai, T. Wang and R.W. Martin, Nanotechnol. 24, 365704 (2013).
- <sup>20</sup> P. Shields, M. Hugues, J. Zúñiga-Pérez, M. Cooke, M. Dineen, W. Wang, F. Causa, and D. Allsopp, phys. Stat. sol. (c), 9, 631 (2012).
- <sup>21</sup> C.C.S. Chan, B.P.L. Reid, R.A. Taylor, Y.D. Zhuang, P.A. Shields, D.W.E. Allsopp, and W. Jia, Appl. Phys. Lett. 102, 111906 (2013).
- <sup>22</sup> J. Bruckbauer, P. R. Edwards, T. Wang and R. W. Martin, Appl. Phys. Lett **98**, 141908 (2011).
- M. Hugues, P.A. Shields, F. Sacconi, M. Mexis, M. Auf der Maur, M. Cooke, M. Dineen, A. Di Carlo, D.W.E. Allsopp, and J. Zúñiga-Pérez, J. Appl. Phys. 114, 084307 (2013).
- <sup>24</sup> Y. Kawakami, A. Kaneta, L. Su, Y. Zhu, K. Okamoto, M. Funato, A. Kikuchi and K. Kishino, J. Appl. Phys. **107**, 023522 (2010).
- <sup>25</sup> D. Drouin, A. R. Couture, D. Joly, X. Tastet, V. Aimez and R. Gauvin, Scanning 29, 92 (2007).